Chemical Engineering Journal 472 (2023) 145121

Contents lists available at ScienceDirect

Chemical Engineering Journal

journal homepage: www.elsevier.com/locate/cej

Investigating the stretchability of doped poly(3-hexylthiophene)-*block*-poly (butyl acrylate) conjugated block copolymer thermoelectric thin films

Qing-Bao Zheng [a], Yan-Cheng Lin [b,f,*], Yen-Ting Lin [a], Yun Chang [a], Wei-Ni Wu [a], Jhih-Min Lin [c], Shih-Huang Tung [d], Wen-Chang Chen [e,f], Cheng-Liang Liu [a,f,*]

[a] Department of Materials Science and Engineering, National Taiwan University, Taipei 10617, Taiwan
[b] Department of Chemical Engineering, National Cheng Kung University, Tainan 70101, Taiwan
[c] National Synchrotron Radiation Research Center, Hsinchu 30076, Taiwan
[d] Institute of Polymer Science and Engineering, National Taiwan University, Taipei 10617, Taiwan
[e] Department of Chemical Engineering, National Taiwan University, Taipei 10617, Taiwan
[f] Advanced Research Center for Green Materials Science and Technology, National Taiwan University, Taipei 10617, Taiwan

ARTICLE INFO

Keywords:
Thermoelectric
Stretchable
Block copolymer
Doping
Polythiophene

ABSTRACT

Organic-based thermoelectric materials have become increasingly popular for their ability to convert waste heat into electricity, coupled with their low processing costs, mechanical flexibility, and non-toxicity, making them an attractive option for wearable electronics. However, there is a lack of direct integration of intrinsically stretchable semiconducting polymers in wearable thermoelectric devices. This study investigates the potential of using poly(3-hexylthiophene)-*block*-poly(butyl acrylate) (P3HT-*b*-PBA) copolymers doped with 2,3,5,6-tetrafluoro-7,7,8,8-tetracyanoquinodimethane (F4TCNQ) to develop stretchable thermoelectric devices. Two PBA block lengths, with number molecular weights (M_n) of 3,000 and 6,000, were compared to pristine P3HT homopolymer. We found that all films exhibited edge-on orientations before and after doping, as determined by GIWAXS analysis. The lamellar distance increases while the $\pi - \pi$ stacking distance decreases upon doping, indicating that the dopants preferentially allocate in the side-chain domain. Accordingly, the optimized power factor (*PF*) of the doped P3HT-*b*-PBA_{3k} and P3HT-*b*-PBA_{6k} films are found to be 2.13 and 1.42 μW m^{-1} K^{-2}, respectively; and the stretchable thermoelectric device comprising P3HT-*b*-PBA_{3k} and a poly(dimethylsiloxane) (PDMS) substrate demonstrate good stretchability with a high *PF* of 1.77 μW m^{-1} K^{-2} at 50% strain, and a high *PF* retention 86.3% relative *PF* after 200 stretch/release cycles. This outstanding performance highlights the feasibility of fabricating stretchable thermoelectric device by using intrinsically stretchable semiconducting polymer. The study presents a promising approach for creating stretchable thermoelectric devices using conjugated/insulating block copolymers combining the thermoelectric properties of P3HT and the intrinsic softness of PBA.

1. Introduction

As the demand for sustainable energy sources continues to increase, there is growing interest in the development of thermoelectric materials that can convert waste heat into electricity [1–5]. Organic thermoelectric materials offer several advantages over their inorganic counterparts, including low processing costs, mechanical flexibility, and non-toxicity [6–19]. The performance of thermoelectric materials is typically determined by their *ZT* values ($ZT = S^2\sigma T/\kappa$), which is a function of the electrical conductivity (σ), Seebeck coefficient (S), thermal conductivity (κ), and absolute temperature (T) [20,21]. In the case of organic thermoelectric materials, the low κ of polymers is typically exploited to optimize the power factor (*PF*), which is given by $PF = S^2\sigma$. However, achieving an optimal balance between the σ and S is essential to improving the overall *PF* [22–24]. Molecular doping is a widely used approach to control the carrier concentration of conjugated polymers to improve their thermoelectric properties [25–29]. This approach involves charge transfer between the polymer and the dopant, which can modify the σ and S, and *PF* of the thermoelectric materials [25,30–32]. Among the various conjugated polymers, polythiophene have been

* Corresponding authors at: Department of Chemical Engineering, National Cheng Kung University, Tainan 70101, Taiwan (Y. Lin); Department of Materials Science and Engineering, National Taiwan University, Taipei 10617, Taiwan (C. Liu).
E-mail addresses: ycl@gs.ncku.edu.tw (Y.-C. Lin), liucl@ntu.edu.tw (C.-L. Liu).

https://doi.org/10.1016/j.cej.2023.145121
Received 20 April 2023; Received in revised form 16 July 2023; Accepted 28 July 2023
Available online 29 July 2023
1385-8947/© 2023 Elsevier B.V. All rights reserved.

extensively studied due to their compatibility with a range of different dopants. Examples of such dopants include ferric chloride ($FeCl_3$) [33–36], gold chloride ($AuCl_3$) [34], ferric triflate [$Fe(OTf)_3$] [33], 2,3,5,6-tetrafluoro-7,7,8,8-tetracyaniquinodimethane (F4TCNQ) [35,37] and others [33,36].

Stretchable organic electronics have shown great potential for next-generation wearable electronics due to their ability to maintain electrical properties during various mechanical deformations and their good adhesion to non-planar-shaped surfaces [38]. While various types of stretchable organic electronic devices [39] such as transistors [40,41], light-emitting diodes [42,43], sensors [44–46], and energy storage devices [47,48] have been widely investigated, stretchable organic thermoelectric devices have not received as much attention. To address this gap, researchers have proposed several strategies to fabricate stretchable organic thermoelectric devices with high performance, including molecular structure engineering, blending with elastic materials, and adopting elastomer substrates [38]. For example, Li et al. enhanced the thermoelectric and mechanical performance of PEDOT/LiTFSI hybrid stretchable films by utilizing the modulation effect of an ionic liquid, resulting in nearly two orders of magnitude increase in *S* and *PF* [49]. The modulation of ionic liquid improves the continuity of PEDOT and rearranges the cross-linked polymer chains, which in turn contributes to the 21% tensile strain of the PEDOT:PSS film. Taroni et al. blended PEDOT:PSS with elastomeric polyurethane to fabricate freestanding and stretchable PEDOT:PSS-based thermoelectric films, achieving a remarkable breaking strain of ~700% without destroying the *S* (~15 μV K^{-1}) [50]. Jeong et al. treated PEDOT:PSS ink with polyethylene glycol (PEG) on a prestrained PDMS film to increase σ without deteriorating thermoelectric performance [51]. Upon releasing the strain, an undulated surface formed without compromising the thermoelectric performance. However, further research is needed into stretchable organic thermoelectric materials that can maintain their thermoelectric properties under high strains. Therefore, our objective is to explore the current state-of-the-art stretchable polymeric thermoelectric materials by fundamental structural engineering and highlight the potential of block polymers for future research in this field [52,53]. The notable advantages of the block polymers include: (i) improving the stretchability by maintaining crystallinity in a fiber-like morphology; (ii) avoiding the formation of a macroscopic vertically phase-separated structure when blending with elastomers, and a microphase separation conferred by using self-assembled block copolymers will be beneficial for thermal conduction and thermoelectric output; (iii) copolymerization of block copolymers enables to have good characteristics of homogeneous distribution, showing better and more uniform doping effects.

In this work, we present a promising approach to create stretchable polymer-based thermoelectric devices using thin films of poly(3-hexylthiophene)-*block*-poly(butyl acrylate) (P3HT-*b*-PBA) copolymers [54] vapor-doped with F4TCNQ [37], where two PBA length with molecular weights of 3,000 and 6,000 in block copolymers were compared to P3HT homopolymer. We investigate the optimal doping conditions, and the specific doping duration to achieve the highest thermoelectric performance. Furthermore, we fabricate the thermoelectric films on a poly (dimethylsiloxane) (PDMS) substrates to demonstrate its stretchability under high strain levels. Characterization of the doped polymer films is conducted using optical absorption spectroscopy, 2D grazing-incidence wide-angle X-ray scattering (2D-GIWAXS), X-ray photoelectron spectroscopy (XPS), and ultraviolet photoelectron spectroscopy (UPS). Our results demonstrate that the F4TCNQ-doped P3HT-*b*-PBA_{3k} film can maintain a high *PF* of 1.77 μW m^{-1} K^{-2} under 50% strain and retain 86.3% relative *PF* after 200 stretch/release cycles. This study provides valuable insights into the development of stretchable organic thermoelectric materials with good thermoelectric properties under high strains.

2. Experimental Section

2.1. Materials

Click reaction between alkynyl-terminated poly(3-hexylthiophene) and azido-terminated poly(butyl acrylate) was performed to synthesize poly(3-hexylthiophene)-*block*-poly(butyl acrylate) conjugated diblock copolymers (P3HT-*b*-PBA), according to our previous report [55]. The alkynyl-terminated P3HT, P3HT-*b*-PBA_{3k} (number average molecular weight (M_n) of PBA ~3000) and P3HT-*b*-PBA_{6k} (M_n of PBA ~6000), with the constant molecular weight of P3HT block (M_n ~ 10,000) and varying lengths of PBA block, were used to investigate how the lengths of soft PBA chain affect the physical properties and TE performance. Moreover, according to our previous report [53], the elastic moduli for P3HT and P3HT-*b*-PBA_{3k} are 930 and 630 MPa, respectively, showing that the enhanced ductility achieved by introduction the low glass transition temperature of PBA chain into the rigid and crystalline P3HT block.

The relevant structures are illustrated in Fig. 1a. All solvents used in this work, including chloroform (CF, anhydrous, 99.9%), chlorobenzene (CB, anhydrous, 99.8%), and isopropanol (IPA), were purchased from Sigma-Aldrich, while 2,3,5,6-tetrafluoro-7,7,8,8-tetracyaniquinodimethane (F4TCNQ) was purchased from Tokyo Chemical Industry Co., Ltd. All chemicals were used as received and without further purification.

2.2. Thermoelectric film fabrication and measurement

The fabrication procedure for polymer thermoelectric thin film doped with F4TCNQ is schematically illustrated in Fig. S1. First, glass substrates were thoroughly cleaned in the ultrasonic bath with deionized water, acetone, and isopropanol for 10 min each and then dried before use. Next, the polythiophene films were prepared under an N_2-filled glove box via spin-coating onto the UV/O_3-treated glass substrates at 1000 rpm for 60 s from 10 mg mL^{-1} polymer solution in CF. The polymer films were then annealed at 50 °C for 2 h and then cooled to room temperature. Sequential doping with F4TCNQ was achieved via heating evaporation. The F4TCNQ powder was placed in a glass bottle, and the bottle was heated at 230 °C to induce sublimation towards the polymer samples on top for various exposure durations spanning the range of 1 to 2, 3, 4, and 5 min [56,57]. The resulting doped polymer films had a thickness of approximately 100 nm, as determined by using the stylus profiler.

A PDMS slab was prepared by casting a standard mixture of 10-part base elastomer and 1-part curing agent, which could be used as the stretchable substrate. To remove any air bubbles, the mixing container was placed under a vacuum for 25 min and then in an oven at 60 °C for 24 hr. The PDMS was modified by immersing it in a non-polar CB solvent and then dipping it in a less polar solvent IPA for 30 s to remove contaminants and modify the surface energy of the PDMS substrates, allowing the polymer films to be deposited on the PDMS surface [58]. The polymer thin film fabrication method was the same as that used for the glass substrates.

The *S* and σ were measured simultaneously using a commercial ZEM-3 measurement system (ADVANCE RIKO Inc., Japan). Silver paste contact was deposited on both ends of the samples prior to measurement to reduce the contact resistance at the electrodes. The measurement was carried out in a helium atmosphere at reduced pressure under 303 K with three different temperature gradients. The polymer/PDMS samples were stretched under different strain levels spanning the range of 25% to 100%.

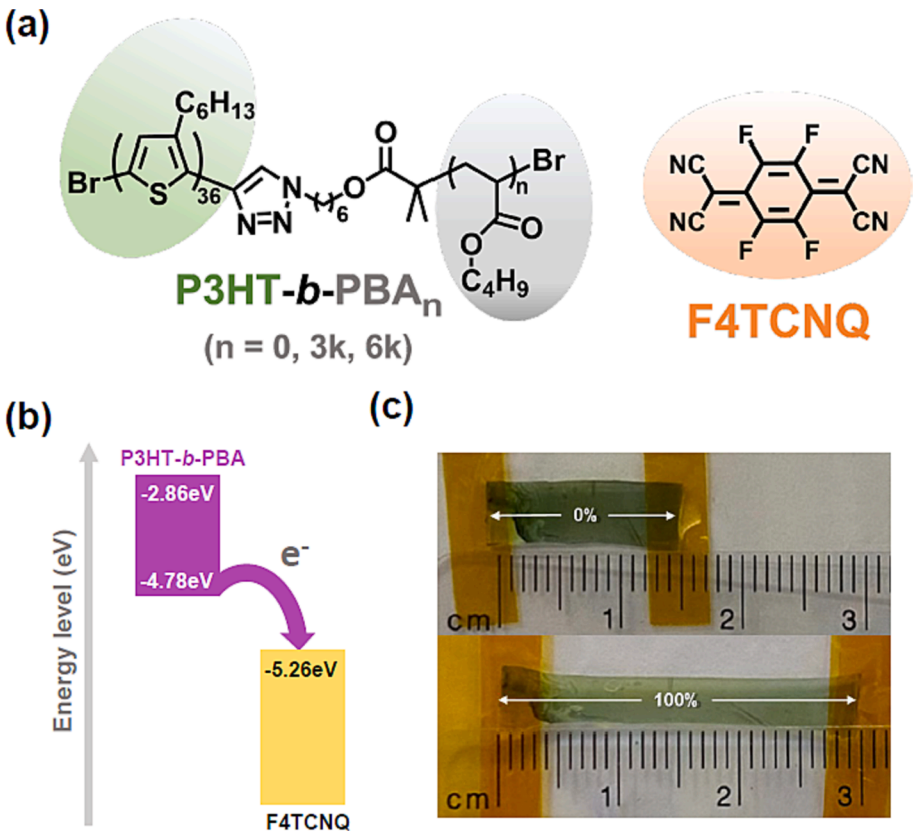

Fig. 1. (a) Chemical structures of P3HT-*b*-PBA block copolymer and F4TCNQ dopant. (b) Energy level diagram and the schematic of p-type doping of P3HT-*b*-PBA and F4TCNQ. (c) Photographs showing the stretching of the thermoelectric film on a PDMS support at 100% strains.

3. Results and discussion

3.1. Thermoelectric properties

In Fig. 1a, the molecular structures of three polythiophenes and a dopant used in the study are illustrated. Two block copolymers, P3HT-*b*-PBA_{3k} and P3HT-*b*-PBA_{6k}, containing a P3HT conjugated block and a PBA coil block, were selected as model materials for stretchable thermoelectric devices referring to their previous use in stretchable transistor applications [55]. The reference of P3HT homopolymer was also investigated to compare its performance with those of block copolymers. To improve the intrinsic σ of the P3HT-*b*-PBA block copolymers, a molecular dopant of F4TCNQ was used to dope the thin films. The HOMO and LUMO energy levels of P3HT-*b*-PBA_{3k} and P3HT-*b*-PBA_{6k} copolymers were comparable, with values of approximately −4.7 eV and −2.8 eV, respectively [55]. By sequential evaporation doping of F4TCNQ to the spin-coated polymer films, the dopant molecule then accepts an electron from the conjugated polymers. P-type doping of thermoelectric polymers with the good doping ability of F4TCNQ is a widely used system where an electron is donated from HOMO of P3HT-*b*-PBA to LUMO of F4TCNQ, leading to an integer charge transfer (Fig. 1b). Optical photographs of the doped P3HT-*b*-PBA_{3k} film on PDMS before and after stretching are shown in Fig. 1c, indicating that the film did not show obvious crack even at 100% strain.

We first conducted the thermoelectric properties of F4TCNQ-doped P3HT-*b*-PBA films by considering the various PBA composition. The intrinsic electrical properties would be different depending on the composition of block copolymer and the resultant microstructures, and the mobility of block copolymers became lower with the increase of PBA coil length [55]. Therefore, the length of PBA may cause different thermoelectric properties during the vapor doping process. The doped samples were prepared by sequential vapor doping, and Ag paste was used to improve the electrical contact. The thermoelectric properties were then characterized at 303 K in an inert helium atmosphere, and the thermoelectric parameters were measured with the samples on the glass substrate. Prior to the systematic studies, the optimal vapor doping time was determined. Fig. 2 depicts the thermoelectric parameters (*S*, σ, and *PF*) for doped P3HT-*b*-PBA_{3k} and P3HT-*b*-PBA_{6k} film as a function of the vapor doping duration. The results show that the doping duration significantly affects the conductivity but does not vary the *S* so much. The σ of the doped P3HT-*b*-PBA_{3k} and P3HT-*b*-PBA_{6k} first increases and then decreases as the doping duration increases from 1 to 5 min, with maximal σ of 5.46 and 3.77 S cm^{-1} after 2 and 3 min vapor doping, respectively. In contrast, the *S* remains steady at 60–70 μV K^{-1}. Therefore, the *PF* follows a similar trend with σ, with a maximum value of 2.13 and 1.42 μW m^{-1} K^{-2} for P3HT-*b*-PBA_{3k} and P3HT-*b*-PBA_{6k} film at the doping time of 2 and 3 min, respectively. Accordingly, P3HT-*b*-PBA with a shorter length of PBA block yields a higher *PF* primary from its enhanced σ. It was also found that the doped P3HT-*b*-PBA_{3k} film reaches the optimal *PF* at a comparatively shorter doping time, suggesting the effective p-doped with F4TCNQ from the increased amount of P3HT block. The doped P3HT homopolymer films achieve σ of 7.88 S cm^{-1} and *S* of 141.1 μV K^{-1}, resulting in an expected higher *PF* of 14.63 μW m^{-1} K^{-2} which is also comparable to the previously reported values based on F4TCNQ-doped P3HT film [59].

3.2. Spectroscopic properties

The normalized solid-state UV − vis − NIR absorption spectra were implemented to characterize the doping behavior of P3HT-*b*-PBA block copolymer and P3HT homopolymer films, as shown in Fig. 3a, b and S2a, respectively. The undoped P3HT-*b*-PBA films show distinct λ_{max} wavelengths at 520 and 545 nm, along with a vibrational peak at 600 nm. These characteristics are similar to those of the P3HT homopolymer,

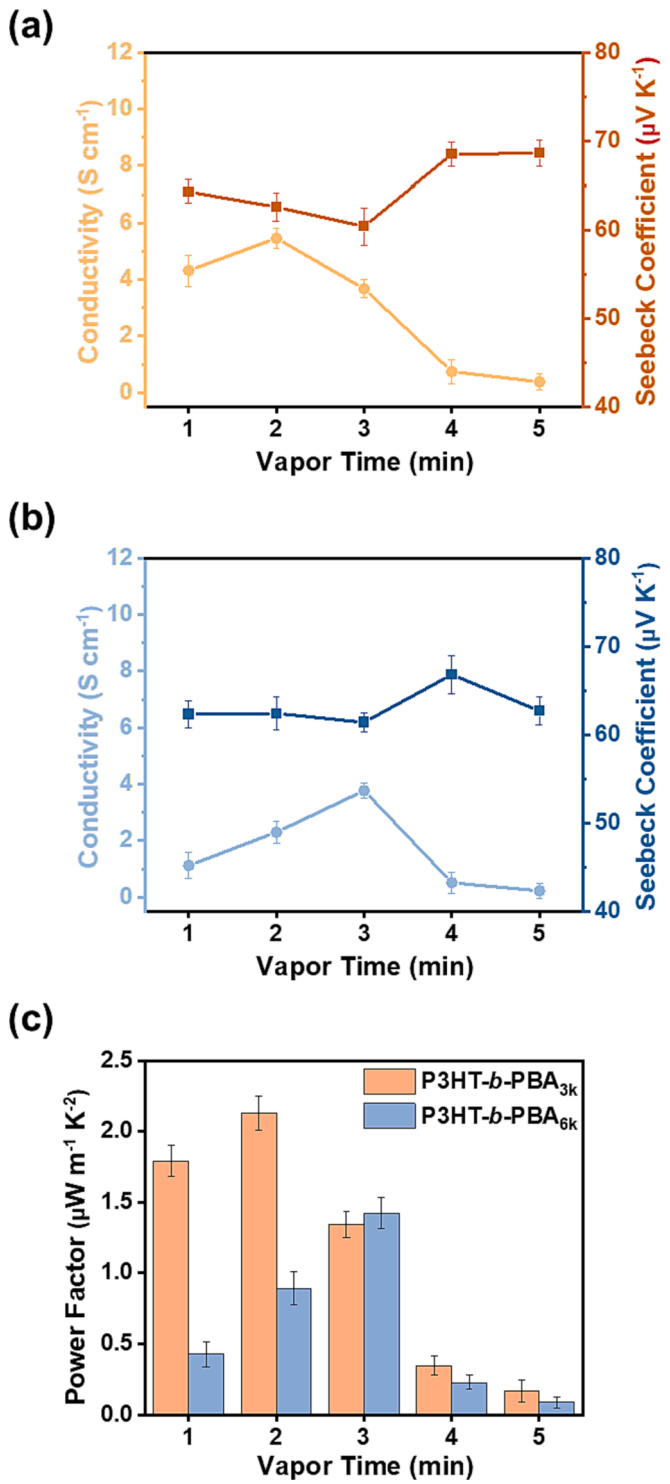

Fig. 2. Conductivity and Seebeck coefficient of (a) P3HT-*b*-PBA$_{3k}$ and (b) P3HT-*b*-PBA$_{6k}$ films with varied vapor-doping durations of F4TCNQ. (c) Power factor of P3HT-*b*-PBA$_{3k}$ and P3HT-*b*-PBA$_{6k}$ films, with varied vapor-doping durations. The conductivity and Seebeck coefficient were collected at 303 K.

suggesting that the flexible PBA coils do not disrupt the interchain packing, as well as the π-π stacking structures of the P3HT block. Upon doping, the peak at approximately 1500 nm appears [60,61], corresponding to the polaronic band, as well as characteristic peaks at 440, 765, and 850 nm, attributed to the F4TCNQ anion, indicating an integer charge transfer doping mechanism [62]. The neutral P3HT peak exhibits a significant decrease following the doping process, while the peaks attributed to the doped state become more prominent.

Fig. 3c, d and S3–S4 depict the changes in the Raman spectrum of P3HT-*b*-PBA thin film upon various doping durations, which are sensitive to the charging of the conjugated thiophene backbone. In the range of 1300 to 1700 cm^{-1}, the undoped P3HT-*b*-PBA presents two characteristic peaks in the Raman spectrum, corresponding to the C − C intra-ring stretching in the thiophene ring at 1380 cm^{-1} and C = C symmetric stretching at 1450 cm^{-1} [63]. Upon vapor doping by F4TCNQ, the peak associated with the C = C symmetric stretching broadens and shifts toward lower energy, down to 1437 cm^{-1}. The broadening of this peak may result from the presence of differently ordered and charged P3HT chains in the film, combined with feature peaks of the neutral polymer and F4TCNQ [64]. The appearance of the red-shifted band corresponds to the increased conformational order of polymer chains, indicating the structural transition of the P3HT block from benzoid to quinoid form [65]. Furthermore, a new Raman peak observed at 1642 cm^{-1} indicates the formation of the F4TCNQ anion. Overall, the Raman spectra reveal that the introduction of dopants into the P3HT-*b*-PBA film was traced, in which the additional polarons are the main charge carriers at this doping level. These findings are consistent with previous reports on chemically doped P3HT film shown in S2b [66].

3.3. Morphological and microstructural analysis

The morphology of vapor-doped P3HT-*b*-PBA films was characterized by atomic force microscopy (AFM), as shown in Figs. S5 and S6. The pristine films of both P3HT-*b*-PBA$_{3k}$ and P3HT-*b*-PBA$_{6k}$ exhibited a nanofiber structure that is potentially conducive to the charge transport process. This morphology is similar to the P3HT homopolymer film due to the low PBA ratio in P3HT-b-PBA$_{3k}$. After vapor-doping, AFM images show only F4TCNQ crystal aggregation on the surface of polymers films [57].

To gain further insights into the molecular packing and crystallinity behavior of the doped P3HT-*b*-PBA films, 2D grazing-incidence wide-angle X-ray scattering (GIWAXS) was implemented. Fig. 4 and Figs. S7 and S8 track the morphological evolution in 2D-GIWAXS of P3HT-*b*-PBA polymers before and after doping. The microstructural arrangements within the crystalline film regions also gain further insight into their thermoelectric performance. The distance in the side chain stacking and π − π stacking was assigned as (*h*00) and (0 1 0) along the q_{xy} (in-plane) and q_z (out-of-plane) direction, respectively. The strong (*h*00) peaks represent the lamellar stacking along the out-of-plane direction, demonstrating a preferential crystalline edge-on orientation. Moreover, the dominated edge-on orientations were observed in the P3HT-*b*-PBA films before and after doping, preserving the crystalline microstructure of the undoped films [67,68]. Notably, among the vapor-doped P3HT-*b*-PBA films, the lamellar spacing increases while the π − π stacking distance decreases upon doping, indicating that the dopants prefer to allocate in the side chain domains of the polymer without disrupting the microstructure. Then, the lamellar spacing and π − π stacking distance stopped increasing when there was insufficient space both in amorphous and crystalline domains to accommodate additional dopants molecular. Consequently, the F4TCNQ molecules started to form crystals on the surface. Accumulation of neat F4TCNQ crystals was observed from the appearance of additional scattering patterns in doped samples heavily under prolonged F4TCNQ doping, which may deteriorate the σ of the films. Therefore, the P3HT-*b*-PBA$_{3k}$ and P3HT-*b*-PBA$_{6k}$ films receiving 2 and 3 min vapor-doping produce slightly increased lamellar spacing in conjunction with the maximal σ of 5.46 and 3.77 S cm^{-1}, respectively. These results are in good accordance with the thermoelectric properties that demonstrate the relationship between σ, morphologies, and molecular packing structures of P3HT-*b*-PBA films.

3.4. UPS and XPS spectra

After investigating the morphology of the vapor-doped P3HT-*b*-PBA

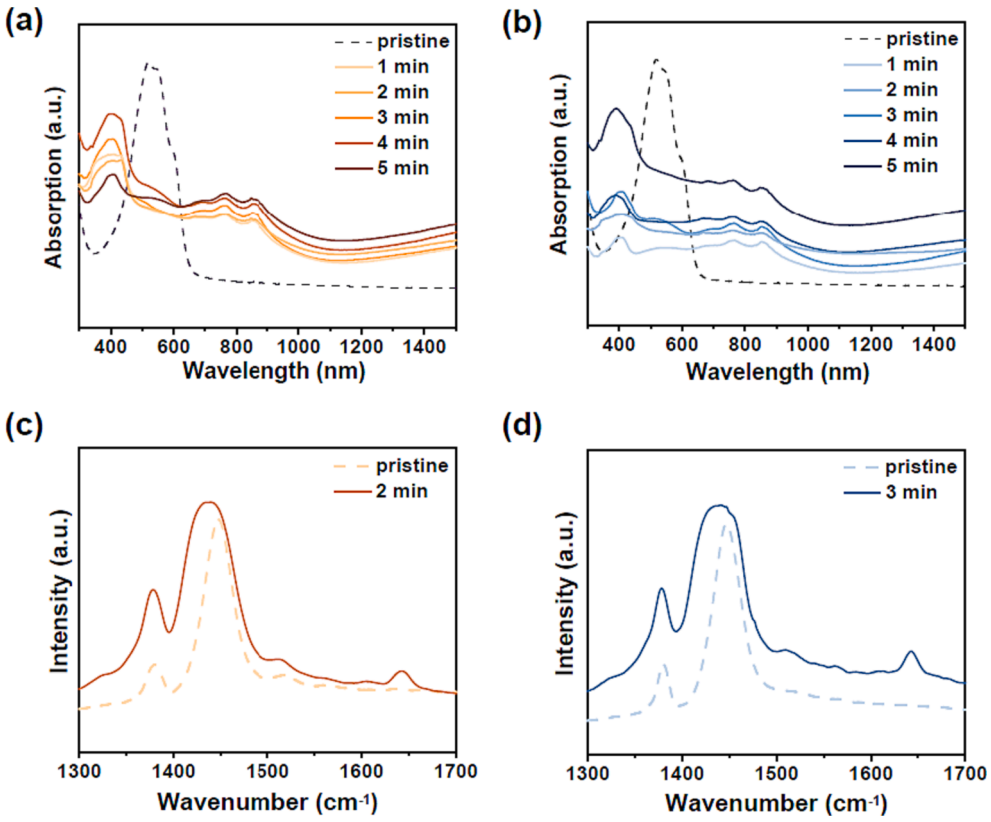

Fig. 3. (a,b) UV–vis–NIR absorption spectrum and (c,d) Raman spectrum of the pristine and the vapor-doped (a,c) P3HT-*b*-PBA_{3k} and (b,d) P3HT-*b*-PBA_{6k} films.

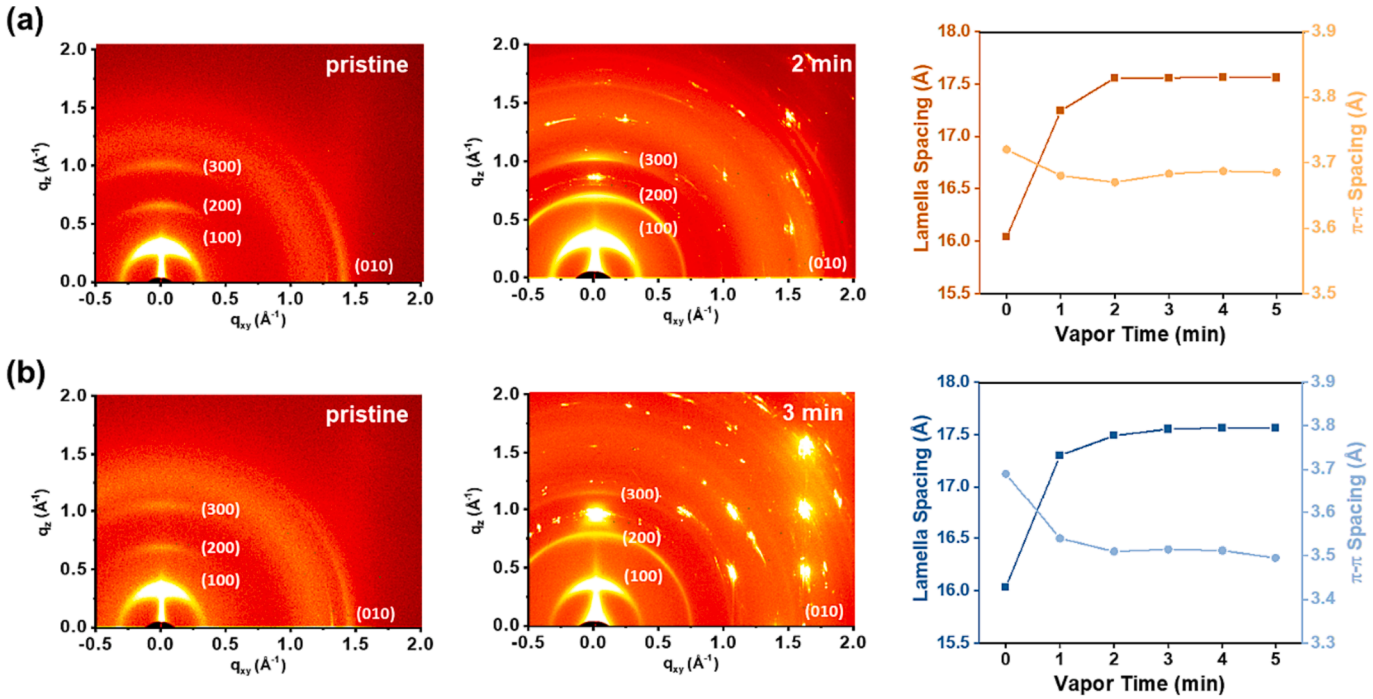

Fig. 4. The lamellar distance extracted from out-of-plane profiles of 2D GIWAXS patterns for the pristine and the vapor-doped (a) P3HT-*b*-PBA_{3k} and (b) and P3HT-*b*-PBA_{6k} films.

films, their optical properties are subsequently characterized. Here, we described the results of the ultraviolet photoelectron spectroscopy (UPS) and X-ray photoelectron spectroscopy (XPS) measurements for P3HT-*b*-PBA films doped with F4TCNQ. UPS spectra were used to study the shift of Fermi level (E_f) and work function (φ) of the doped films compared to the undoped films for the optimal *PF* conditions, while XPS spectra were used to identify the S 2p peak and the N 1 s peaks and their binding energies before and after doping. The UPS spectra presented in Fig. 5a, b

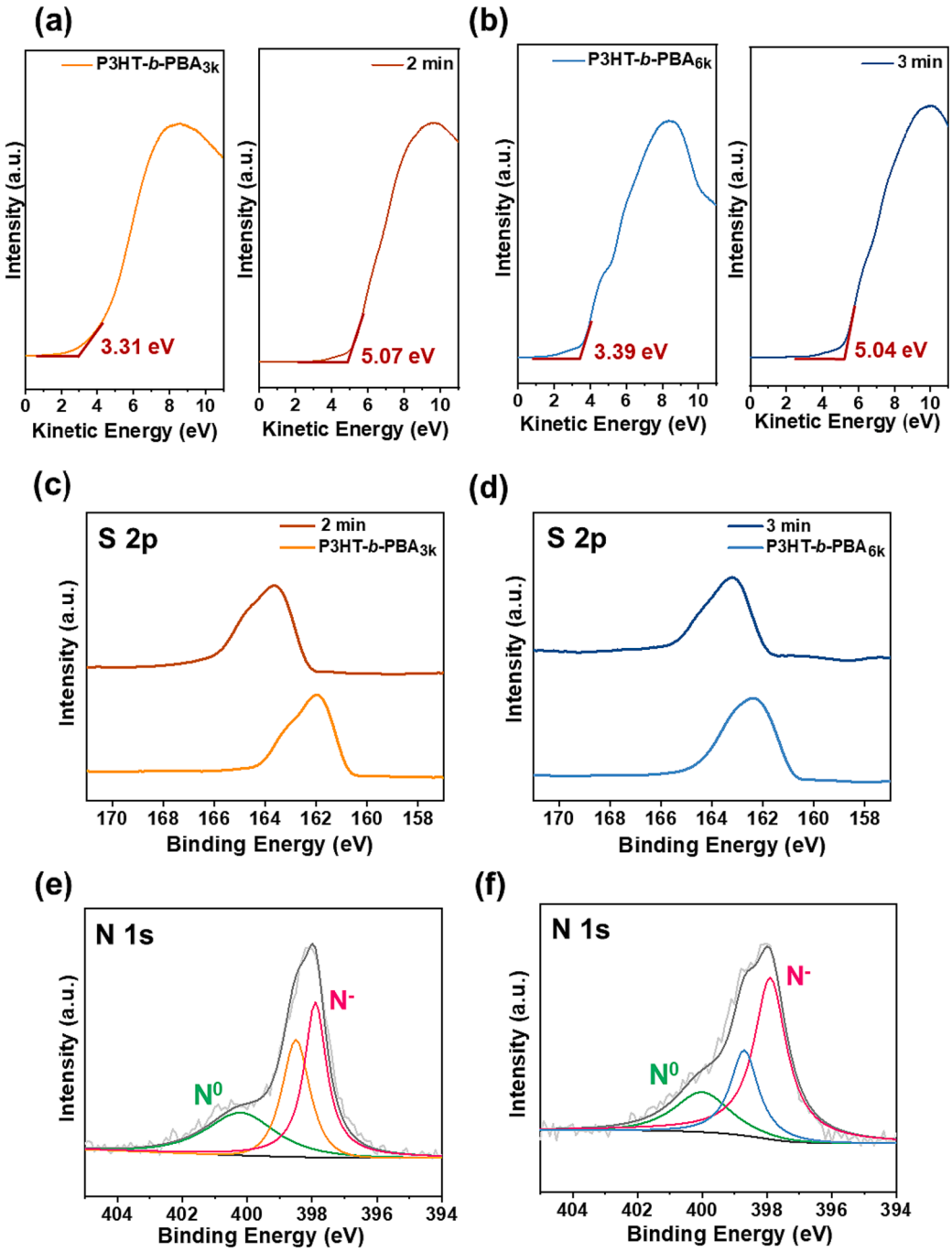

Fig. 5. UPS spectra for the secondary electron cut-off region and work function with/without vapor doping: (a) pristine P3HT-*b*-PBA$_{3k}$, (b) doped P3HT-*b*-PBA$_{3k}$, (c) pristine P3HT-*b*-PBA$_{6k}$ and (d) doped P3HT-*b*-PBA$_{6k}$ films. XPS spectra of S 2p and N 1 s peaks for doped films of (e) P3HT-*b*-PBA$_{3k}$ and (f) P3HT-*b*-PBA$_{6k}$.

show that the φ of the doped P3HT-*b*-PBA$_{3k}$ and P3HT-*b*-PBA$_{6k}$ films increases from 3.31 and 3.39 eV to 5.07 and 5.04 eV, respectively, compared to the pristine films, indicating a shift of E_f towards the HOMO energy level. This is typically observed in a p-type doping process [69]. Moreover, P3HT-*b*-PBA$_{3k}$ presents a larger shift of φ than that of P3HT-*b*-PBA$_{6k}$, indicating a higher doping level achieved by P3HT-*b*-PBA$_{3k}$. This is advantageous for improving thermoelectric performance. The XPS measurements of P3HT-*b*-PBA films were performed at the optimal vapor doping duration to determine the highest *PF* and compare with their analogs before doping.

The XPS spectra (Fig. 5c and d) of the undoped P3HT-*b*-PBA films showed a S 2p peak at binding energies of ~162.3 eV [70]. The XPS spectra showed a shift in the S 2p peak of P3HT-*b*-PBA films upon doping with F4TCNQ, indicating a decrease in the electron density of the S atom in the thiophene moiety of P3HT-*b*-PBA film, which suggests that the S atom is involved in the doping process and acts as an electron-donating associate. The neutral N 1 s peak of the undoped P3HT-*b*-PBA appeared at binding energy of ~398.3 eV (Fig. S9). In addition, the new N 1 s peak arising from adding the F4TCNQ molecules was observed in the XPS spectra (Fig. 5e and f) [71]. Previous studies have shown that there are two doping mechanisms of F4TCNQ: integer charge transfer (ICT) and charge transfer complexation (CTC), which can be assigned to an ionized N^{-1} peak (~397.6 eV) and a neutral N^0 peak (~399.5 eV), respectively [72,73]. Among them, ICT is beneficial for increasing the conductivity since it generates free carriers in the polymer via charge transfer to F4TCNQ. ICT involves an electron transfer to the F4TCNQ molecule,

which results in a higher electron density and a shift to lower binding energies. Therefore, the doping efficiency (η_d) of the F4TCNQ-doped P3HT-*b*-PBA films was then calculated by the following equation:

$$\eta_d = \frac{A^{-1}}{A^0 + A^{-1}} \quad (1)$$

where A^0 and A^{-1} are the areas of the N^0 and N^{-1} peaks, respectively [57]. The η_d of the F4TCNQ vapor-doped P3HT-*b*-PBA_{3k} and P3HT-*b*-PBA_{6k} films was found to be 75.9% and 60.7%, respectively, which is consistent with the higher σ and the corresponding *PF* of the vapor-doped P3HT-*b*-PBA_{3k} film.

3.5. Strain-dependent thermoelectric characteristics of doped block copolymer film

Here, we further conducted a study to investigate the ductility of F4TCNQ-doped P3HT-*b*-PBA_{3k} films at their optimal power output conditions. Thermoelectric devices were prepared on a PDMS substrate, and the thermoelectric properties at strain levels from 0 to 100% were analyzed (Fig. 6a and b). It was observed that the σ decreased while the *S* increased as the strain level increased. The declining trend of the *PF* was similar to σ since the σ is a more dominant factor than *S*. Compared to the doped P3HT films, the combination of PBA blocks indeed enhanced the overall mechanical endurance of the films and maintained the semiconducting/thermoelectric properties of P3HT blocks, as shown in Fig. 6c and d. At 50% strain, the σ and *PF* of the F4TCNQ-doped P3HT films decreased by 97% and 95%, respectively; and the film could not stretch beyond this point. In stark contrast, the F4TCNQ-doped P3HT-*b*-PBA_{6k} produced much higher performance than their analog of P3HT under strains. In addition, the σ of the F4TCNQ-doped P3HT-*b*-PBA_{6k} films decreased more slowly than P3HT-*b*-PBA_{3k} films at higher strain levels, which may be due to the larger ratio of PBA block promoting the stretchability of the thermoelectric films. Despite the drop in σ and *PF*, the doped P3HT-*b*-PBA_{3k} films still presented higher σ values than that of P3HT films under the same strain. This improvement indicates that the balance between stretchability and high thermoelectric properties can be achieved by optimizing the block ratio in the P3HT-*b*-PBA film.

Optical microscopy images of the surface structure of the doped P3HT, P3HT-*b*-PBA_{3k}, and P3HT-*b*-PBA_{6k} films under mechanical strains were also characterized (Fig. 7). Upon the application of strain, microscale cracks were observed from the P3HT films at 25% strain, which continued to enlarge with increasing strain. In contrast, P3HT-*b*-PBA_{3k} films exhibited only a few cracks perpendicular to the strain direction at 50% strain, while P3HT-*b*-PBA_{6k} films maintained smooth surfaces even at 100% strain. This suggests that the ductility of the P3HT-*b*-PBA films was significantly improved by incorporating PBA into the conjugated block polymers, and this improved stretchability as further characterized by using 2D GIWAXS (Fig. 8a and b and Figs. S10 and S1). As can be seen, the (200) and (300) lamellar signals of the doped films became weaker with increasing tensile strain, and the thermoelectric properties also became worse under higher strain conditions. Fig. 8c and d summarizes the lamellar and π-π spacing under different levels of strain, revealing similar trends for all films when subjected to 50% strain. Lamellar spacing slightly decreased due to a compression of the layer-by-layer lamellar stacking, where the strain direction is perpendicular to the lamellar stacking direction. However, as the tensile strain increased to 50–100%, lamellar spacing of the doped P3HT-*b*-PBA_{3k} films recovered to their original state, possibly due to crack formation releasing the tensile strain in the stretched film. However, for doped P3HT-*b*-PBA_{6k} films, the lamellar spacing distance continued to decrease as no obvious cracks occurred on the surface, which could endure the strain. Meanwhile, the π-π distance which is parallel to the stretching direction, increased under 0–50% for doped P3HT-*b*-PBA_{3k} and P3HT-*b*-PBA_{6k} films. Similarly, as tensile strain increased to 50–100%, the π-π distance for doped P3HT-*b*-PBA_{6k} films kept increasing while the doped P3HT-*b*-PBA_{3k} films slightly decreased.

Finally, endurance tests of the stretchable thermoelectric devices were stretched in the air for different stretching/releasing cycles and measured by the ZEM-3 instrument to track the thermoelectric parameters including *S* and σ. Accordingly, the F4TCNQ-doped P3HT-*b*-PBA_{3k} and P3HT-*b*-PBA_{6k} films were cycled at 50% strain for 500 cycles and the results are shown in Fig. S12. After 200 cycles, the *PF* retention for the F4TCNQ-doped P3HT-*b*-PBA_{3k} and P3HT-*b*-PBA_{6k} films were 83.3% and 86.3%, respectively; and they remained at 56.3% and 57.9% after 500 cycles, showing their reproducibility and stability. According to the literature on the design of stretchable conductive polymers [74], it is noted that the balancing stretchability and electrical performance is a challenging aspect to address in structural design. Therefore, stretchable thermoelectric devices can be realized by using intrinsically stretchable P3HT-*b*-PBA by using molecular doping and optimizing the block ratio

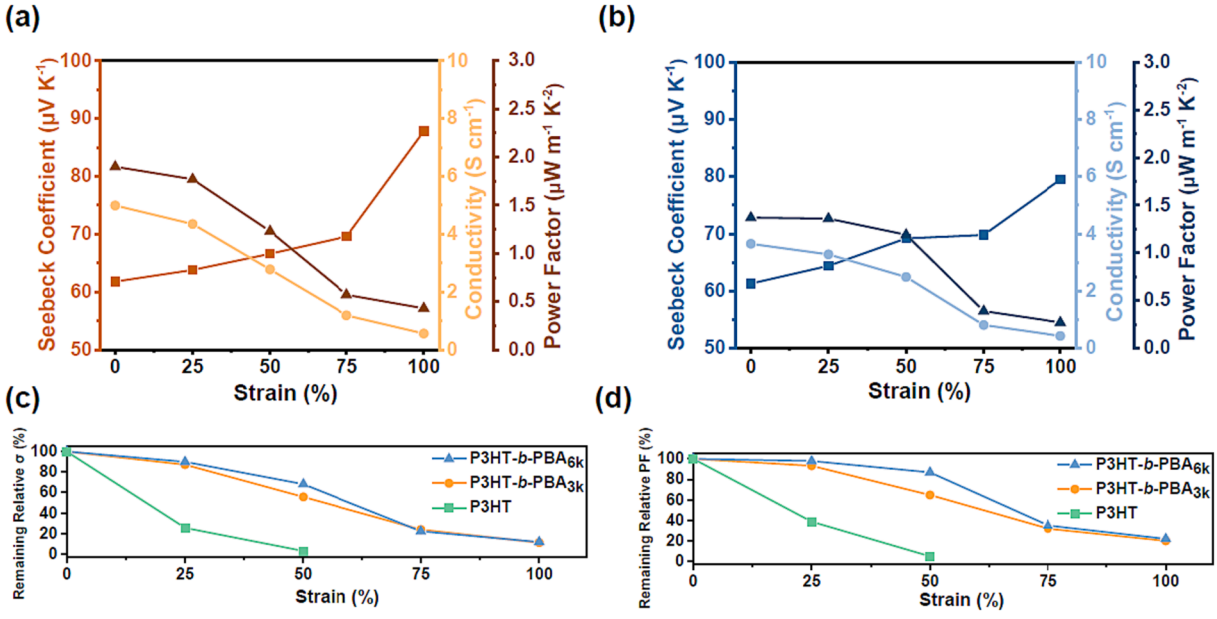

Fig. 6. Thermoelectric performances of the vapor-doped (a) P3HT-*b*-PBA_{3k} (2 min) and (b) P3HT-*b*-PBA_{6k} films (3 min) under varied strain levels spanning the range of 0–100%. Retentions of (c) σ and (d) *PF* of the vapor-doped P3HT-*b*-PBA_{3k}, P3HT-*b*-PBA_{6k} films and their analog of P3HT under different strain levels.

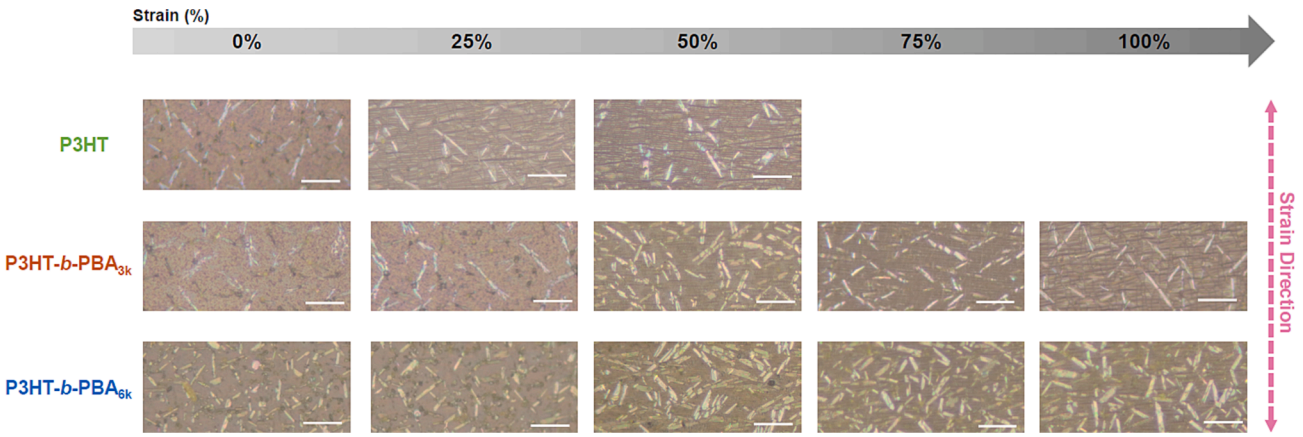

Fig. 7. Optical microscopy images of the optimized vapor-doped P3HT-*b*-PBA_{3k} and P3HT-*b*-PBA_{6k} films and their analog of P3HT under different strain levels; the inset scale bars represent 20 μm.

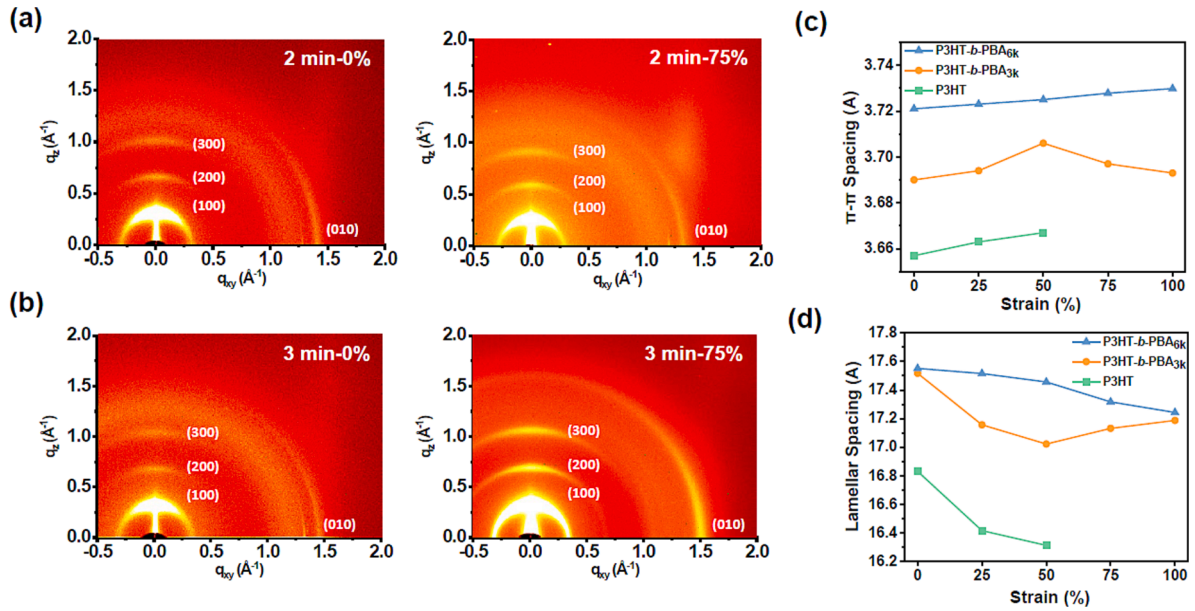

Fig. 8. 2D GIWAXS profiles of the vapor-doped (a) P3HT-*b*-PBA_{3k} and (b) P3HT-*b*-PBA_{6k} with optimized doping duration at 75% strain. (c) Lamellar spacing and (d) $\pi-\pi$ stacking distance of the vapor-doped P3HT-*b*-PBA_{3k} and P3HT-*b*-PBA_{6k} films and their analog of P3HT under varied strain levels. Note that the crystallographic parameters were extracted from 2D GIWAXS profiles with the incident beam perpendicular to the strain direction.

to strike a balance between the stretchability and the thermoelectric performance.

On the other hand, tests on the blended systems were also performed to compare with the block copolymers in this study. To elucidate the comprehensive comparison, we have conducted additional the experiments on blended P3HT/PBA films, directly mixing PBA (M_n = 3000 g/mol) and P3HT (M_n = 10,000 g/mol) under the same processing condition of P3HT-*b*-PBA films as described in our Experimental Section. Upon examining the OM images (Fig. S13), it is evident that the blended P3HT/PBA films exhibit an apparent inhomogeneous surface, even after one day of stirring. This surface morphology contrasts with the smooth surface observed in the block copolymer thin film. The observed poorer miscibility in the blending system may be attributed to the significant difference in glass transition temperature between P3HT and PBA. Furthermore, when subjected to vapor-doping with F4TCNQ, the resistance of the blended film was too large to be accurately measured, indicating that the insulating nature of PBA hindered the formation of a continuous charge transport pathway. These results clearly demonstrate that the block copolymer system is more suitable for thermoelectric devices compared to the direct blending of a conjugated polymer and a rubber.

4. Conclusion

In summary, our study focused on fabricating F4TCNQ-doped P3HT-*b*-PBA conjugated block copolymers thin films for use in stretchable TE applications. The P3HT and PBA blocks were molecularly engineered to be responsible for semiconducting properties and mechanical endurance, respectively; and the films were attached to elastomeric PDMS substrates to improve their overall stretchability. The F4TCNQ-doped P3HT-*b*-PBA_{3k} films showed the highest *PF* value of 2.13 μW m^{-1} K^{-2} after receiving 2 min of vapor doping, which is accompanied by the increased lamellar spacing distance due to the accommodation of molecular dopants. The doping efficiency of F4TCNQ in P3HT-*b*-PBA_{3k} was found to be 1.3 times higher than P3HT-*b*-PBA_{6k} based on XPS analysis. The doped P3HT-*b*-PBA_{3k} film spin-coated on PDMS substrate could maintain 83% *PF* under 50% strain and 86.3% relative *PF* after 200 stretch/release cycles, indicating promising stability and stretchability.

Overall, our results present a new route for fabricating stretchable polymeric thin films that maintain good thermoelectric performance under high strain up to 100%, with potential applications in wearable thermoelectric generators [75,76].

Declaration of Competing Interest

The authors declare the following financial interests/personal relationships which may be considered as potential competing interests: Cheng-Liang Liu reports financial support was provided by National Science and Technology Council.

Data availability

Data will be made available on request.

Acknowledgments

The authors acknowledge the financial support from 2030 Cross-Generation Young Scholars Program by the National Science and Technology Council (NSTC) in Taiwan under grant 111-2628-E-002-014 and 112-2628-E-002-013, Academic Research-Career Development Project (Sprout Research Projects) by National Taiwan University (NTU112L7856), and Advanced Research Center for Green Materials Science and Technology from The Featured Area Research Center Program within the framework of the Higher Education Sprout Project by the Ministry of Education (112L9006). The authors also thank Beamline TPS 25A at National Synchrotron Radiation Research Center (NSRRC) of Taiwan for providing beamtime.

Appendix A. Supplementary data

Supplementary data to this article can be found online at https://doi.org/10.1016/j.cej.2023.145121.

References

[1] X.L. Shi, J. Zou, Z.G. Chen, Advanced thermoelectric design: from materials and structures to devices, Chem. Rev. 120 (2020) 7399–7515, https://doi.org/10.1021/acs.chemrev.0c00026.
[2] M. Massetti, F. Jiao, A.J. Ferguson, D. Zhao, K. Wijeratne, A. Wurger, J. L. Blackburn, X. Crispin, S. Fabiano, Unconventional thermoelectric materials for energy harvesting and sensing applications, Chem. Rev. 121 (2021) 12465–12547, https://doi.org/10.1021/acs.chemrev.1c00218.
[3] W.-Y. Chen, X.-L. Shi, J. Zou, Z.-G. Chen, Wearable fiber-based thermoelectrics from materials to applications, Nano Energy 81 (2021), 105684, https://doi.org/10.1016/j.nanoen.2020.105684.
[4] W. Lee, S. Lee, H. Kim, Y. Kim, Organic thermoelectric devices with PEDOT:PSS/ZnO hybrid composites, J. Chem. Eng. 415 (2021), 128935, https://doi.org/10.1016/j.cej.2021.128935.
[5] P.-S. Lin, S. Inagaki, J.-H. Liu, M.-C. Chen, T. Higashihara, C.-L. Liu, The role of branched alkylthio side chain on dispersion and thermoelectric properties of regioregular polythiophene/carbon nanotubes nanocomposites, J. Chem. Eng. 458 (2023), 141366, https://doi.org/10.1016/j.cej.2023.141366.
[6] Y. Chen, Y. Zhao, Z. Liang, Solution processed organic thermoelectrics: towards flexible thermoelectric modules, Energy Environ. Sci. 8 (2015) 401–422, https://doi.org/10.1039/c4ee03297g.
[7] R. Kroon, D.A. Mengistie, D. Kiefer, J. Hynynen, J.D. Ryan, L. Yu, C. Muller, Thermoelectric plastics: from design to synthesis, processing and structure-property relationships, Chem. Soc. Rev. 45 (2016) 6147–6164, https://doi.org/10.1039/c6cs00149a.
[8] C.J. Yao, H.L. Zhang, Q. Zhang, Recent progress in thermoelectric materials based on conjugated polymers, Polymer 11 (2019) 107, https://doi.org/10.3390/polym11010107.
[9] L. Deng, Y. Liu, Y. Zhang, S. Wang, P. Gao, Organic thermoelectric materials: niche harvester of thermal energy, Adv. Funct. Mater. 33 (2022) 2210770, https://doi.org/10.1002/adfm.202210770.
[10] C. Zhang, X. Zhu, N-type quinoidal oligothiophene-based semiconductors for thin-film transistors and thermoelectrics, Adv. Funct. Mater. 30 (2020) 2000765, https://doi.org/10.1002/adfm.202000765.
[11] H. Wang, W. Chu, G. Chen, A brief review on measuring methods of thermal conductivity of organic and hybrid thermoelectric materials, Adv. Electron. Mater. 5 (2019) 1900167, https://doi.org/10.1002/aelm.201900167.
[12] Y. Sun, C.A. Di, W. Xu, D. Zhu, Advances in n-type organic thermoelectric materials and devices, Adv. Electron. Mater. 5 (2019) 1800825, https://doi.org/10.1002/aelm.201800825.
[13] E.W. Zaia, M.P. Gordon, P. Yuan, J.J. Urban, Progress and perspective: soft thermoelectric materials for wearable and internet-of-things applications, Adv. Electron. Mater. 5 (2019) 1800823, https://doi.org/10.1002/aelm.201800823.
[14] Y. Jia, Q. Jiang, H. Sun, P. Liu, D. Hu, Y. Pei, W. Liu, X. Crispin, S. Fabiano, Y. Ma, Y. Cao, Wearable thermoelectric materials and devices for self-powered electronic systems, Adv. Funct. Mater. 33 (2021) 2102990, https://doi.org/10.1002/adma.202102990.
[15] Y. Wang, L. Yang, X.L. Shi, X. Shi, L. Chen, M.S. Dargusch, J. Zou, Z.G. Chen, Flexible thermoelectric materials and generators: challenges and innovations, Adv. Funct. Mater. 31 (2019) 1807916, https://doi.org/10.1002/adma.201807916.
[16] J. Wang, L. Liu, F. Wu, Z. Liu, Z. Fan, L. Chen, Y. Chen, Recent developments of n-type organic thermoelectric materials: influence of structure modification on molecule arrangement and solution processing, ChemSusChem 15 (2022) 202102420, https://doi.org/10.1002/cssc.202102420.
[17] S. Wang, G. Zuo, J. Kim, H. Sirringhaus, Progress of conjugated polymers as emerging thermoelectric materials, Prog. Polym. Sci. 129 (2022), 101548, https://doi.org/10.1016/j.progpolymsci.2022.101548.
[18] D. Zhou, H. Zhang, H. Zheng, Z. Xu, H. Xu, H. Guo, P. Li, Y. Tong, B. Hu, L. Chen, Recent advances and prospects of small molecular organic thermoelectric materials, Small 18 (2022) 2200679, https://doi.org/10.1002/smll.202200679.
[19] Y. Xu, Y. Jia, P. Liu, Q. Jiang, D. Hu, Y. Ma, Poly(3,4-ethylenedioxythiophene) (PEDOT) as promising thermoelectric materials and devices, J. Chem. Eng. 404 (2021), 126552, https://doi.org/10.1016/j.cej.2020.126552.
[20] H. Wang, C. Yu, Organic thermoelectrics: materials preparation, performance optimization, and device integration, Joule 3 (2019) 53–80, https://doi.org/10.1016/j.joule.2018.10.012.
[21] K.A. Peterson, E.M. Thomas, M.L. Chabinyc, Thermoelectric properties of semiconducting polymers, Annual Review of Materials Research 50 (2020) 551–574, https://doi.org/10.1146/annurev-matsci-082219-024716.
[22] E.H. Suh, M.K. Jeong, K. Lee, W. Jeong, J. Jang, I.H. Jung, Solution-state doping-assisted molecular ordering and enhanced thermoelectric properties of an amorphous polymer, Int. J. Energy Res. 45 (2021) 21540–21551, https://doi.org/10.1002/er.7266.
[23] Q. Zhang, Y. Sun, W. Xu, D. Zhu, What to expect from conducting polymers on the playground of thermoelectricity: lessons learned from four high-mobility polymeric semiconductors, Macromolecules 47 (2014) 609–615, https://doi.org/10.1021/ma4020406.
[24] B. Russ, A. Glaudell, J.J. Urban, M.L. Chabinyc, R.A. Segalman, Organic thermoelectric materials for energy harvesting and temperature control, Nat. Rev. Mater. 1 (2016) 1–14, https://doi.org/10.1038/natrevmats.2016.50.
[25] W. Zhao, J. Ding, Y. Zou, C.A. Di, D. Zhu, Chemical doping of organic semiconductors for thermoelectric applications, Chem. Soc. Rev. 49 (2020) 7210–7228, https://doi.org/10.1039/d0cs00204f.
[26] A. Tripathi, Y. Lee, S. Lee, H.Y. Woo, Recent advances in n-type organic thermoelectric materials, dopants, and doping strategies, J. Mater. Chem. C 10 (2022) 6114, https://doi.org/10.1039/d1tc06175e.
[27] T.L.D. Tam, J. Xu, Strategies and concepts in n-doped conjugated polymer thermoelectrics, J. Mater. Chem. A 9 (2021) 5149–5163, https://doi.org/10.1039/d0ta12166e.
[28] J. Min Han, S. Eun Yoon, K. Hyun Jung, O. Bae, D. Kim, U. Kim, H. Seo, F. Sunjoo Kim, K. Chul Kim, J.H. Kim, B.-G. Kim, Dopant-dependent thermoelectric performance of indoloindole-selenophene based conjugated polymer, J Chem. Eng. 431 (2022), 133779, https://doi.org/10.1016/j.cej.2021.133779.
[29] J. Wu, X. Yin, F. Yang, S. Wang, Y. Liu, X. Mao, X. Nie, S. Yang, C. Gao, L. Wang, Improving the thermoelectric performances of polymer via synchronously realizing of chemical doping and side-chain cleavage, J. Chem. Eng. 429 (2022), 132354, https://doi.org/10.1016/j.cej.2021.132354.
[30] A.D. Scaccabarozzi, A. Basu, F. Anies, J. Liu, O. Zapata-Arteaga, R. Warren, Y. Firdaus, M.I. Nugraha, Y. Lin, M. Campoy-Quiles, N. Koch, C. Muller, L. Tsetseris, M. Heeney, T.D. Anthopoulos, Doping approaches for organic semiconductors, Chem. Rev. 122 (2022) 4420–4492, https://doi.org/10.1021/acs.chemrev.1c00581.
[31] J.T. Li, T. Lei, Recent progress on addressing the key challenges in organic thermoelectrics, Chem Asian J 16 (2021) 1508–1518, https://doi.org/10.1002/asia.202100285.
[32] F. Zhang, C.-A. Di, Exploring thermoelectric materials from high mobility organic semiconductors, Chem. Mater. 32 (2020) 2688–2702, https://doi.org/10.1021/acs.chemmater.0c00229.
[33] L. Wu, H. Li, H. Chai, Q. Xu, Y. Chen, L. Chen, Anion-dependent molecular doping and charge transport in ferric salt-doped P3HT for thermoelectric application, ACS Appl. Electron. Mater. 3 (2021) 1252–1259, https://doi.org/10.1021/acsaelm.0c01067.
[34] Y.H. Kang, S.-J. Ko, M.-H. Lee, Y.K. Lee, B.J. Kim, S.Y. Cho, Highly efficient and air stable thermoelectric devices of poly(3-hexylthiophene) by dual doping of Au metal precursors, Nano Energy 82 (2021), 105681, https://doi.org/10.1016/j.nanoen.2020.105681.
[35] Z. Liao, S. Wang, C. Gao, L. Wang, Combining chemical doping and thermal annealing to optimize the thermoelectric performance of the poly(3-hexylthiophene), Compos. Commun. 34 (2022), 101255, https://doi.org/10.1016/j.coco.2022.101255.
[36] Z. Liang, Y. Zhang, M. Souri, X. Luo, A.M. Boehm, R. Li, Y. Zhang, T. Wang, D.-Y. Kim, J. Mei, S.R. Marder, K.R. Graham, Influence of dopant size and electron affinity on the electrical conductivity and thermoelectric properties of a series of

conjugated polymers, J. Mater. Chem. A 6 (2018) 16495–16505, https://doi.org/10.1039/c8ta05922e.
[37] J. Hynynen, D. Kiefer, C. Muller, Influence of crystallinity on the thermoelectric power factor of P3HT vapour-doped with F4TCNQ, RSC Adv. 8 (2018) 1593–1599, https://doi.org/10.1039/c7ra11912g.
[38] Y. Hao, X. He, L. Wang, X. Qin, G. Chen, J. Yu, Stretchable thermoelectrics: strategies, performances, and applications, Adv. Funct. Mater. 32 (2021) 2109790, https://doi.org/10.1002/adfm.202109790.
[39] S.J. Benight, C. Wang, J.B.H. Tok, Z. Bao, Stretchable and self-healing polymers and devices for electronic skin, Prog. Polym. Sci. 38 (2013) 1961–1977, https://doi.org/10.1016/j.progpolymsci.2013.08.001.
[40] M. Ashizawa, Y. Zheng, H. Tran, Z. Bao, Intrinsically stretchable conjugated polymer semiconductors in field effect transistors, Prog. Polym. Sci. 100 (2020), 101181, https://doi.org/10.1016/j.progpolymsci.2019.101181.
[41] S. Wang, J. Xu, W. Wang, G.N. Wang, R. Rastak, F. Molina-Lopez, J.W. Chung, S. Niu, V.R. Feig, J. Lopez, T. Lei, S.K. Kwon, Y. Kim, A.M. Foudeh, A. Ehrlich, A. Gasperini, Y. Yun, B. Murmann, J.B. Tok, Z. Bao, Skin electronics from scalable fabrication of an intrinsically stretchable transistor array, Nature 555 (2018) 83–88, https://doi.org/10.1038/nature25494.
[42] J.H. Koo, D.C. Kim, H.J. Shim, T.-H. Kim, D.-H. Kim, Flexible and stretchable smart display: materials, fabrication, device design, and system integration, Adv. Funct. Mater. 28 (2018) 1801834, https://doi.org/10.1002/adfm.201801834.
[43] Z. Zhang, W. Wang, Y. Jiang, Y.X. Wang, Y. Wu, J.C. Lai, S. Niu, C. Xu, C.C. Shih, C. Wang, H. Yan, L. Galuska, N. Prine, H.C. Wu, D. Zhong, G. Chen, N. Matsuhisa, Y. Zheng, Z. Yu, Y. Wang, R. Dauskardt, X. Gu, J.B. Tok, Z. Bao, High-brightness all-polymer stretchable LED with charge-trapping dilution, Nature 603 (2022) 624–630, https://doi.org/10.1038/s41586-022-04400-1.
[44] S. Zhao, J. Li, D. Cao, G. Zhang, J. Li, K. Li, Y. Yang, W. Wang, Y. Jin, R. Sun, C. P. Wong, Recent advancements in flexible and stretchable electrodes for electromechanical sensors: strategies, materials, and features, ACS Appl. Mater. Interfaces 9 (2017) 12147–12164, https://doi.org/10.1021/acsami.6b13800.
[45] M. Amjadi, K.-U. Kyung, I. Park, M. Sitti, Stretchable, skin-mountable, and wearable strain sensors and their potential applications: a review, Adv. Funct. Mater. 26 (2016) 1678–1698, https://doi.org/10.1002/adfm.201504755.
[46] X. Fan, W. Nie, H. Tsai, N. Wang, H. Huang, Y. Cheng, R. Wen, L. Ma, F. Yan, Y. Xia, PEDOT:PSS for flexible and stretchable electronics: modifications, strategies, and applications, Adv. Sci. 6 (2019) 1900813, https://doi.org/10.1002/advs.201900813.
[47] Z. Zhao, K. Xia, Y. Hou, Q. Zhang, Z. Ye, J. Lu, Designing flexible, smart and self-sustainable supercapacitors for portable/wearable electronics: from conductive polymers, Chem. Soc. Rev. 50 (2021) 12702–12743, https://doi.org/10.1039/d1cs00800e.
[48] Y. Wang, Y. Ding, X. Guo, G. Yu, Conductive polymers for stretchable supercapacitors, Nano Res. 12 (2019) 1978–1987, https://doi.org/10.1007/s12274-019-2296-9.
[49] Q. Li, M. Deng, S. Zhang, D. Zhao, Q. Jiang, C. Guo, Q. Zhou, W. Liu, Synergistic enhancement of thermoelectric and mechanical performances of ionic liquid LiTFSI modulated PEDOT flexible films, J. Mater. Chem. C 7 (2019) 4374–4381, https://doi.org/10.1039/c9tc00310j.
[50] P.J. Taroni, G. Santagiuliana, K. Wan, P. Calado, M. Qiu, H. Zhang, N.M. Pugno, M. Palma, N. Stingelin-Stutzman, M. Heeney, O. Fenwick, M. Baxendale, E. Bilotti, Toward stretchable self-powered sensors based on the thermoelectric response of PEDOT:PSS/polyurethane blends, Adv. Funct. Mater. 28 (2018) 1704285, https://doi.org/10.1002/adfm.201704285.
[51] M.H. Jeong, A. Sanger, S.B. Kang, Y.S. Jung, I.S. Oh, J.W. Yoo, G.H. Kim, K.J. Choi, Increasing the thermoelectric power factor of solvent-treated PEDOT:PSS thin films on PDMS by stretching, J. Mater. Chem. A 6 (2018) 15621–15629, https://doi.org/10.1039/c8ta03606c.
[52] S. Chen, H. Zheng, X. Liu, J. Peng, Tailoring Co-crystallization over Microphase Separation in Conjugated Block Copolymers via Rational Film Processing for Field-Effect Transistors, Macromolecules 55 (2022) 10405–10414, https://doi.org/10.1021/acs.macromol.2c02048.
[53] Y. Yin, S. Chen, S. Zhu, L. Li, D. Zhai, D. Huang, J. Peng, Tailoring Cocrystallization and Microphase Separation in Rod-Rod Block Copolymers for Field-Effect Transistors, Macromolecules 54 (2021) 4571–4581, https://doi.org/10.1021/acs.macromol.0c02788.
[54] B.X. Dong, Z. Liu, J.W. Onorato, T. Ma, J. Strzalka, P. Bennington, C.K. Luscombe, C.K. Ober, P.F. Nealey, S.N. Patel, Ionic dopant-induced ordering enhances the thermoelectric properties of a polythiophene-based block copolymer, Adv. Funct. Mater. 31 (2021) 2106991, https://doi.org/10.1002/adfm.202106991.
[55] J.-T. Wang, S. Takshima, H.-C. Wu, C.-C. Shih, T. Isono, T. Kakuchi, T. Satoh, W.-C. Chen, Stretchable conjugated rod–coil poly(3-hexylthiophene)-block-poly(butyl acrylate) thin films for field effect transistor applications, Macromolecules 50 (2017) 1442–1452, https://doi.org/10.1021/acs.macromol.6b02722.
[56] E. Lim, K.A. Peterson, G.M. Su, M.L. Chabinyc, Thermoelectric properties of poly(3-hexylthiophene) (P3HT) doped with 2,3,5,6-tetrafluoro-7,7,8,8-tetracyanoquinodimethane (F4TCNQ) by vapor-phase infiltration, Chem. Mater. 30 (2018) 998–1010, https://doi.org/10.1021/acs.chemmater.7b04849.
[57] J. Min, D. Kim, S.G. Han, C. Park, H. Lim, W. Sung, K. Cho, Position-induced efficient doping for highly doped organic thermoelectric materials, Adv. Electron. Mater. 8 (2021) 2101142, https://doi.org/10.1002/aelm.202101142.
[58] A. Mohapatra, A. Singh, S.A. Abbas, Y.-J. Lu, K.M. Boopathi, C. Hanmandlu, N. Kaisar, C.-H. Lee, C.-W. Chu, Bilayer polymer solar cells prepared with transfer printing of active layers from controlled swelling/de-swelling of PDMS, Nano Energy 63 (2019), 103826, https://doi.org/10.1016/j.nanoen.2019.06.022.
[59] M.T. Fontana, D.A. Stanfield, D.T. Scholes, K.J. Winchell, S.H. Tolbert, B. J. Schwartz, Evaporation vs solution sequential doping of conjugated polymers: F4TCNQ doping of micrometer-thick P3HT films for thermoelectrics, J. Phys. Chem. C 123 (2019) 22711–22724, https://doi.org/10.1021/acs.jpcc.9b05069.
[60] E.H. Suh, Y.J. Jeong, J.G. Oh, K. Lee, J. Jung, Y.S. Kang, J. Jang, Doping of donor-acceptor polymers with long side chains via solution mixing for advancing thermoelectric properties, Nano Energy 58 (2019) 585–595, https://doi.org/10.1016/j.nanoen.2019.01.075.
[61] D. Kiefer, R. Kroon, A.I. Hofmann, H. Sun, X. Liu, A. Giovannitti, D. Stegerer, A. Cano, J. Hynynen, L. Yu, Y. Zhang, D. Nai, T.F. Harrelson, M. Sommer, A. J. Moule, M. Kemerink, S.R. Marder, I. McCulloch, M. Fahlman, S. Fabiano, C. Muller, Double doping of conjugated polymers with monomer molecular dopants, Nat. Mater. 18 (2019) 149–155, https://doi.org/10.1038/s41563-018-0263-6.
[62] L. Deng, X. Huang, H. Lv, Y. Zhang, G. Chen, Unravelling the mechanism of processing protocols induced microstructure evolution on polymer thermoelectric performance, Appl. Mater. Today 22 (2021), 100959, https://doi.org/10.1016/j.apmt.2021.100959.
[63] N. Chandrasekaran, A. Kumar, L. Thomsen, D. Kabra, C.R. McNeill, High performance as-cast P3HT:PCBM devices: understanding the role of molecular weight in high regioregularity P3HT, Adv. Mater. 2 (2021) 2045–2054, https://doi.org/10.1039/d0ma00738b.
[64] J. Gao, H. Zhai, P. Hu, H. Jiang, The stoichiometry of TCNQ-based organic charge-transfer cocrystals, Cryst. 10 (2020) 993, https://doi.org/10.3390/cryst10110993.
[65] H. Li, J. Song, J. Xiao, L. Wu, H.E. Katz, L. Chen, Synergistically improved molecular doping and carrier mobility by copolymerization of donor–acceptor and donor–donor building blocks for thermoelectric application, Adv. Funct. Mater. 30 (2020) 2004378, https://doi.org/10.1002/adfm.202004378.
[66] M.F. DiTusa, G.L. Grocke, T. Ma, S.N. Patel, Probing the evolution of conductivity and structural changes in vapor-F4TCNQ doped P3HT, Mol. Syst. Des. Eng. 7 (2022) 788–797, https://doi.org/10.1039/d1me00192b.
[67] J.E. Cochran, M.J.N. Junk, A.M. Glaudell, P.L. Miller, J.S. Cowart, M.F. Toney, C. J. Hawker, B.F. Chmelka, M.L. Chabinyc, Molecular interactions and ordering in electrically doped polymers: blends of PBTTT and F4TCNQ, Macromolecules 47 (2014) 6836–6846, https://doi.org/10.1021/ma501547h.
[68] K. Kang, S. Watanabe, K. Broch, A. Sepe, A. Brown, I. Nasrallah, M. Nikolka, Z. Fei, M. Heeney, D. Matsumoto, K. Marumoto, H. Tanaka, S. Kuroda, H. Sirringhaus, 2D coherent charge transport in highly ordered conducting polymers doped by solid state diffusion, Nat. Mater. 15 (2016) 896–902, https://doi.org/10.1038/nmat4634.
[69] B. Li, X. Li, F. Yang, Y. Chen, X. Mao, S. Wan, H. Xin, S. Yan, M. Wang, C. Gao, L. Wang, Enhanced thermoelectric performance of a donor–acceptor-based two-dimensional conjugated polymer with high crystallinity, ACS Appl. Energy Mater. 4 (2021) 4662–4671, https://doi.org/10.1021/acsaem.1c00274.
[70] J.H. Lee, S. Yoon, M.S. Ko, N. Lee, I. Hwang, M.J. Lee, Improved performance of organic photovoltaic devices by doping F4TCNQ onto solution-processed graphene as a hole transport layer, Org. Electron. 30 (2016) 302–311, https://doi.org/10.1016/j.orgel.2016.01.003.
[71] M.P. Gordon, S.A. Gregory, J.P. Wooding, S. Ye, G.M. Su, D.S. Seferos, M. D. Losego, J.J. Urban, S.K. Yee, A.K. Menon, Microstructure and heteroatom dictate the doping mechanism and thermoelectric properties of poly(alkyl-chalcogenophenes), Appl. Phys. Lett. 118 (2021), 233301, https://doi.org/10.1063/5.0052604.
[72] K.E. Watts, B. Neelamraju, E.L. Ratcliff, J.E. Pemberton, Stability of charge transfer states in F4TCNQ-doped P3HT, Chem. Mater. 31 (2019) 6986–6994, https://doi.org/10.1021/acs.chemmater.9b01549.
[73] S.E. Yoon, J. Park, J.E. Kwon, S.Y. Lee, J.M. Han, C.Y. Go, S. Choi, K.C. Kim, H. Seo, J.H. Kim, B.G. Kim, Improvement of electrical conductivity in conjugated polymers through cascade doping with small-molecular dopants, Adv. Funct. Mater. 32 (2020) 2005129, https://doi.org/10.1002/adma.202005129.
[74] J.Y. Oh, S. Rondeau-Gagne, Y.C. Chiu, A. Chortos, F. Lissel, G.N. Wang, B. C. Schroeder, T. Kurosawa, J. Lopez, T. Katsumata, J. Xu, C. Zhu, X. Gu, W.G. Bae, Y. Kim, L. Jin, J.W. Chung, J.B. Tok, Z. Bao, Intrinsically stretchable and healable semiconducting polymer for organic transistors, Nature 539 (2016) 411–415, https://doi.org/10.1038/nature20102.
[75] T. Sun, B. Zhou, Q. Zheng, L. Wang, W. Jiang, G.J. Snyder, Stretchable fabric generates electric power from woven thermoelectric fibers, Nat Commun 11 (2020) 572, https://doi.org/10.1038/s41467-020-14399-6.
[76] Z. Soleimani, S. Zoras, B. Ceranic, Y. Cui, S. Shahzad, A comprehensive review on the output voltage/power of wearable thermoelectric generators concerning their geometry and thermoelectric materials, Nano Energy 89 (2021), 106325, https://doi.org/10.1016/j.nanoen.2021.106325.